Supplementary Information (SI) for Physical Chemistry Chemical Physics.
This journal is © the Owner Societies 2024

Supporting Information

An Orbital-Overlap Complement to σ-Hole Electrostatic Potentials

Arshad Mehmood[a] and Benjamin G. Janesko*[b]

[a] Division of Information Technology - Research Computing, Informatics & Innovation and Institute for Advanced Computational Science, Stony Brook University, Stony Brook, NY 11794, USA.

[b] Department of Chemistry & Biochemistry, Texas Christian University, 2800 South University Drive, Fort Worth, TX 76129, USA.

Corresponding Author

*Email: arshad.mehmood@stonybrook.edu

Phone: +1 631-632-2340

S1. Computational Details

All the calculations for supporting information use the Gaussian 16[1] suite of programs. The coordinates of TM nanoclusters were obtained from Ref. [2] and Ref. [3]. The calculations for these clusters were carried out at PW91PW91[4, 5]/Def2-SV(P)[6, 7] level with effective core potential using the spin states mentioned in those references. The calculations for Figure S5 (Table S2) uses MP2[8]/aug-cc-pVTZ[9] level following Ref. [10]. The Gaussian formatted checkpoint files were used to obtain electron density, ESP, and $D(\vec{r})$ grid data in the Gaussian cube file format using Multiwfn program[11]. For the calculations of $D(\vec{r})$, an even-tempered grid of 50 exponents was used starting from 2.50 $Bohr^{-2}$ and with an increment of 1.50 $bohr^{-2}$. For the studied systems, the calculated ESP and $D(\vec{r})$ cube files were projected over 0.001 $e/bohr^3$ molecular electron density surface. The molecular graphics were created using VMD[12] version 1.9.3 and GaussView 5 package.

S2. Capturing the Effects of Hybridization

The orbital overlap distance measures the size of *orbital lobes*, a property that is *distinct* from the delocalization of orbitals, and polarization of charges and ESP. To illustrate, Figure S1 shows $D(\vec{r})$ for the 1*s*, 2*s*, and 2*p* states of the H atom. $D(\vec{r})$ is modest for the single large lobe of the 1*s* orbital, smaller for the two lobes of the 2*p* orbital, and dominated by the diffuse outer lobe of the 2*s* orbital. This indicates that $D(\vec{r})$ gives information about hybridization; as the atoms with more 2*p* character tend to have smaller $D(\vec{r})$, while atoms with more 2*s* character tend to have larger $D(\vec{r})$.

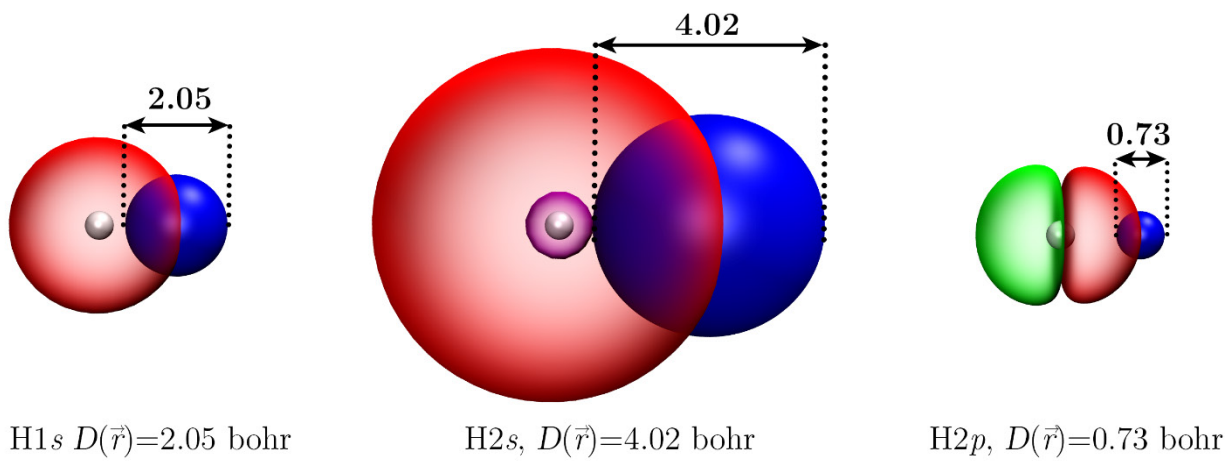

Figure S1 Orbital overlap distance calculated for H atom's 1s (left), 2s (middle) and 2p (right) orbitals. The α-spin orbitals are shown in red and green. The $EDR(\vec{r};d)$ test function shown in blue. The width of test function which maximizes overlap with orbitals to give $D(\vec{r})$ is highlighted for each orbital.

S3. Applications to the Transition Metal Nanoclusters

We extend the applications of the combination of molecular ESP and $D(\vec{r})$ to visualize the σ-holes on transition metals (TM) nanoclusters. The valence configuration of the group IB noble metals, *i.e.* (Cu group), is $d^{10}s^1$ with singly occupied s orbital similar to hydrogen. Upon the formation of the Au_2 cluster, these singly occupied s orbital combine, and their electrons are mainly localized in the bonding region, which creates a positive ESP over the end region along the extension of Au−Au bond as mentioned by Stenlid *et al.*[3] and shown in Figure S2. Since the deficiencies of valence s orbitals induce these positive regions in Cu group metals, therefore, these can be categorized as σ_s-holes. Figure S2 shows that $D(\vec{r})$ in the σ_s-holes regions of Au_2 are distinct from the rest of the molecule, which indicates that $D(\vec{r})$ can capture the σ-holes on transition metals as well. Additionally, the σ_s-holes of Au_2 have large values of $D(\vec{r})$ while the bonding region, which is associated with negative ESP, has small $D(\vec{r})$, implying the former regions are comparatively

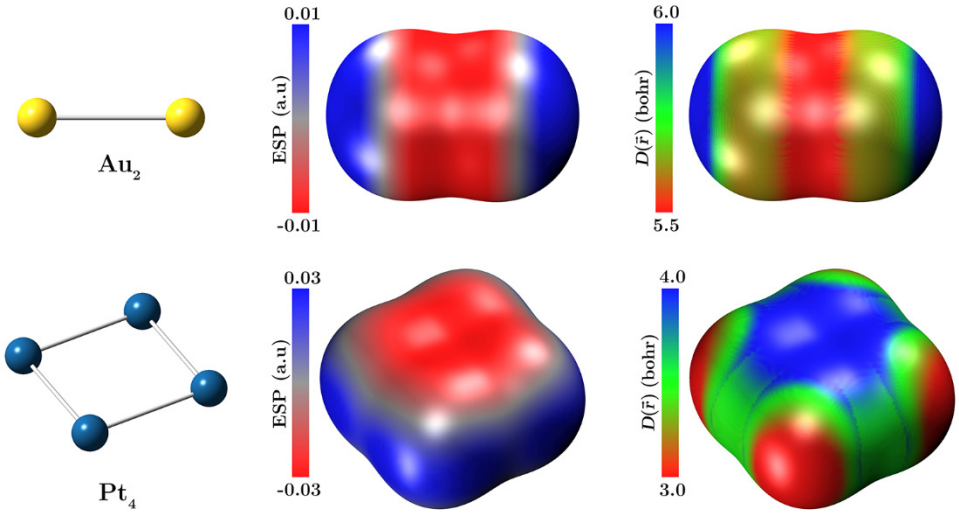

Figure S2. Representative examples of σ_s and σ_d on transition metal nano clusters Au_2 and Pt_4 respectively. The left side of figure shows the gas phase optimized geometry.

diffuse while the latter are compact. Next, consider the example of the Pt_4 cluster. The valence electron configuration of Pt is $5d^9 6s^1$. As reported by Stenlid *et al.*,[2], the formation of Pt_4 creates two types of local ESP positive regions due to the deficiencies of electrons in valence *s* and *d* orbitals, induced by the concentration of electrons from these orbitals to the bonding regions between Pt atoms. The deficiencies in valence *s* orbitals create regions of positive ESP on the corners of Pt_4, which are visible in Figure S2. However, these regions are not associated with ESP maxima. The overlap of $5dz^2$ and $5dx^2$-y^2 creates the deficiencies in *d* orbitals along the extension of the Pt−Pt bonds, which show the local maxima in ESP. These regions thus from σ_d-holes at each side of the corner of Pt_4 square planer structure, as can be seen in Figure S2. In contrast to the Au_2 molecule, the $D(\vec{r})$ plots of Pt_4 cluster are compact at σ_d-holes regions and are diffuse in the hallowed site of the cluster. The compact nature of σ_d-holes can be associated with the compact nature of *d* orbitals relative to the *s* orbitals. However, the $D(\vec{r})$ plot nicely distinguishes the σ_d-holes from the rest of the molecules. To further elaborate on the types and nature of σ-holes on TM nanoclusters, Figure S3 shows the surface plots of ESP and $D(\vec{r})$ for TM_8 clusters of Pt, Ir,

and Au. The surface ESP plots of these nanoclusters follow the previously reported trends of Stenlid *et al.*[2]. For Pt_8 cluster, the ESP maxima are located at three points at the side of each corner Pt atom highlighted using arrows. These points correspond to the extension of each Pt−Pt bond formed by the overlap of $5dz^2$ and $5dx^2$-y^2 (NBO occupation: $5dxy^{1.97}$, $5dxz^{1.97}$, $5dyz^{1.97}$, $5d(x^2-y^2)^{1.56}$, $5d(z^2)^{1.56}$, $6s^{0.75}$, $6p^{0.21}$) orbitals,[2] which creates the *d* orbital electron deficiency at these points and hence provides the examples of σ_d-holes. The $D(\vec{r})$ surface plot of Pt_8 shows maxima

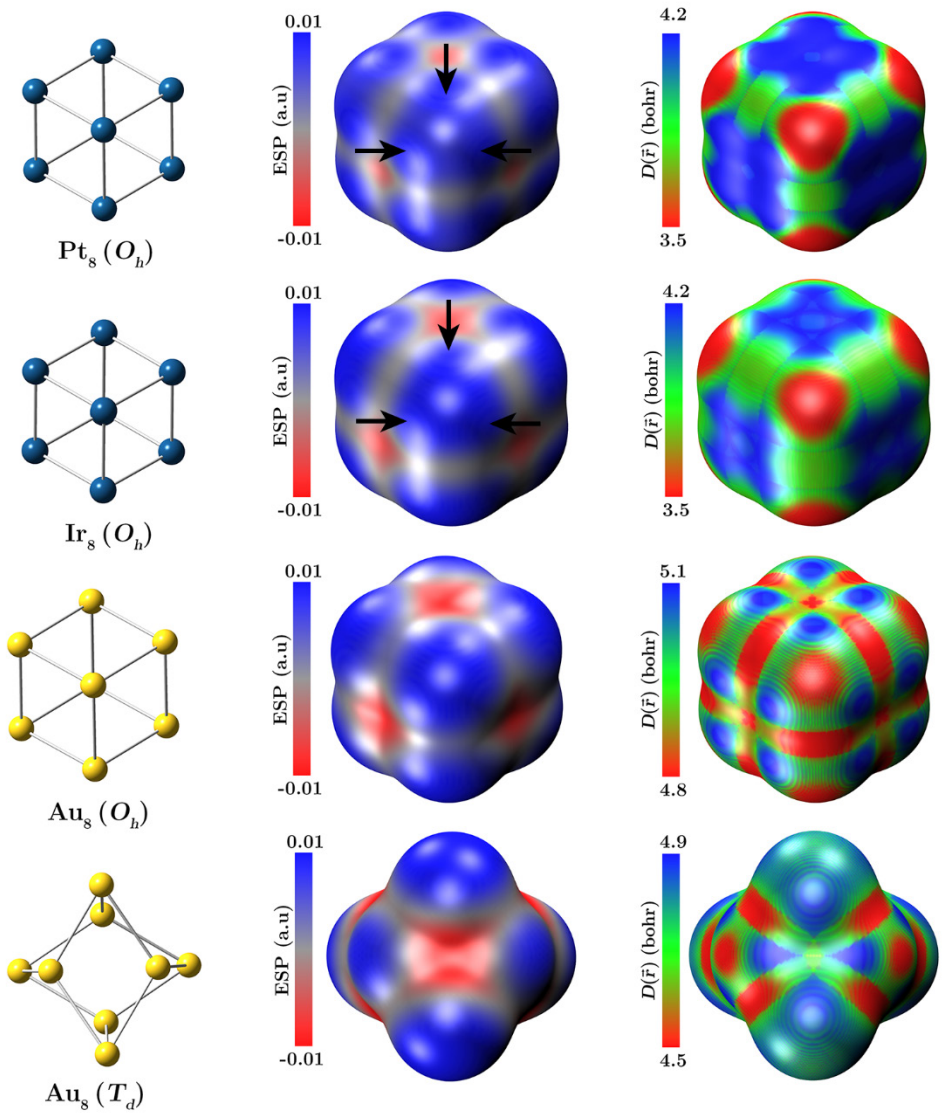

Figure S3. ESP and $D(\vec{r})$ of transition metals Au, Pt and Ir TM_8 nanoclusters in O_h and T_d symmetry. The left side of figure shows the gas phase geometries.

in negative ESP regions, which are located at the interatomic hollow sites. Similar to the Pt_4 clusters, the σ_d-holes regions of Pt_8 are compact compared to the rest of the molecule, as revealed by the small value of $D(\vec{r})$ on these regions. On the other hand, the ESP maxima of Ir_8 are created by the overlap of compact $5dz^2$ and $5dx^2$-y^2 orbitals and relatively diffuse and partially filled remaining $5d$ orbitals (NBO occupation: $5dxy^{1.65}$, $5dxz^{1.65}$, $5dyz^{1.65}$, $5d(x^2- y^2)^{1.51}$, $5d(z^2)^{1.51}$, $6s^{0.75}$, $6p^{0.29}$).[2] This overlap results in a triangular-shaped ESP maximum, *i.e.,* σ_d-holes at each corner of the Ir_8 cluster. The corners of triangular ESP regions are highlighted using arrows in Figure S3. Like the Pt_8 cluster, the $D(\vec{r})$ surface plot is compact at the σ_d-holes sites; however, the magnitude of $D(\vec{r})$ (red color intensity) is smaller as compared to that for Pt_8 cluster. This indicated that $D(\vec{r})$ captures the mixing of relatively diffuse $5d$ orbitals, which was absent in the Pt_8 cluster. For both, O_h and T_d Au_8 clusters, the ESP maxima is located at the corner sites and not along the extension of the Au−Au bond, which contradicts the classical definition of σ-hole. This anomaly is also captured by $D(\vec{r})$ surface plot, which exhibits different behaviors for Au_2 (Figure S2) and Au_8 clusters, e.g., ESP maxima regions for Au_2 and Au_8 (T_d) have a large value of $D(\vec{r})$. In contrast, for Au_8 (O_h), these regions are compact with smaller values of $D(\vec{r})$. To get further insight into the nature of ESP maxima on gold nanoclusters, we extended the study to include large-sized nanoclusters of Au_{13} and Au_{55}.

Figure S4 shows the surface ESP and $D(\vec{r})$ plots of low energy, icosahedral and cuboctahedra Au_{13} nanoclusters. The ESP maxima of these clusters are located at low coordinated atoms.[2] For the low energy Au_{13} cluster, this maximum is positioned at the capping atom, whereas for other Au_{13} clusters, the maxima are located at each corner atom. Similar to the Au_8 clusters these ESP maxima are not positioned along the extension of Au−Au bond but are located at the tips, *i.e.,* on top sites of Au atoms contradicting the definition of a true σ-hole. The $D(\vec{r})$ plots show

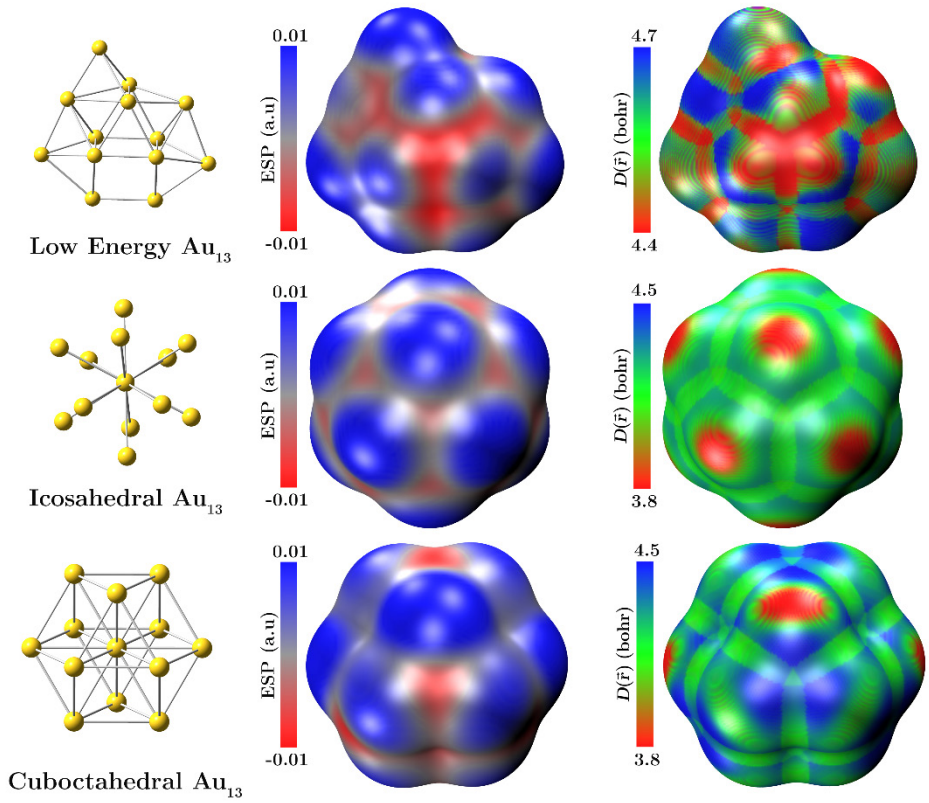

Figure S4. Surface plots of ESP and $D(\vec{r})$ of Au_{13} nanoclusters. The left side of figure shows the gas phase geometries.

the top atom of low energy Au_{13} cluster, which has a maximum value of ESP, is relatively more diffuse as compared to edge atoms which have lower values of ESP. The corner atoms of other Au_{13} clusters, which are associated with ESP maxima, have the smallest values of $D(\vec{r})$, following the trends of other TM nanoclusters of Figure S2 and Figure S3. This trend is also followed in the Au_{55} cluster, except the facet central atoms (highlighted using letter "C" in Figure 5 of the manuscript). Based on these observations, we suggest that the regions of ESP maxima on gold clusters are not σ-holes but show a local polarization in ESP induced by the bond formation. These anomalies of gold clusters have also been reported by Stenlid *et al.,* who used the term pseudo-σ-holes for these regions.[2] These studies establish that the combination of ESP and $D(\vec{r})$ surface plots provide a valuable tool to capture the location and rationalize the relative nature of various types of σ-holes on TM clusters.

Table S1 Calculated surface $D(\vec{r})$ (bohr) and maximum ESP on σ-hole $V_{S,max}$ (a.u) of various σ-hole donors calculated at various levels of theory using def2-QZVP basis sets. The σ-hole is evaluated on the first atom of the molecule named highlighted in red and italic.

Molecule	HF		cam-B3LYP		B3LYP		ωB97XD		CCSD		MP2	
	$D(\vec{r})$	$V_{S,max}$	$D(\vec{r})$	$V_{S,max}$	$D(\vec{r})$	$V_{S,max}$	$D(\vec{r})$	$V_{S,max}$	$D(\vec{r})$	$V_{S,max}$	$D(\vec{r})$	$V_{S,max}$
Cl-Cl	3.20	0.056	3.21	0.052	3.20	0.052	3.20	0.052	3.19	0.052	3.19	0.053
Br-Br	3.29	0.062	3.29	0.059	3.28	0.059	3.29	0.059	3.27	0.058	3.27	0.058
I-I	3.45	0.068	3.43	0.064	3.41	0.063	3.43	0.065	3.42	0.063	3.41	0.061
H-H	3.88	0.028	3.97	0.026	3.95	0.026	3.89	0.026	3.82	0.026	3.84	0.027
Cl-CH_3	3.22	0.006	3.23	0.007	3.22	0.007	3.22	0.006	3.21	0.007	3.21	0.007
Br-CH_3	3.32	0.017	3.32	0.019	3.31	0.019	3.31	0.019	3.30	0.018	3.30	0.017
I-CH_3	3.49	0.035	3.47	0.035	3.46	0.034	3.47	0.035	3.46	0.033	3.45	0.031
H-CH_3	3.28	0.022	3.29	0.022	3.28	0.021	3.28	0.022	3.28	0.022	3.28	0.023
Cl-FCH_2	3.24	0.026	3.25	0.020	3.24	0.024	3.24	0.022	3.23	0.023	3.23	0.023
Br-FCH_2	3.33	0.030	3.33	0.029	3.32	0.028	3.33	0.028	3.31	0.028	3.31	0.036
I-FCH_2	3.52	0.046	3.48	0.044	3.46	0.042	3.48	0.043	3.47	0.042	3.45	0.038
H-FCH_2	3.42	0.046	3.44	0.040	3.43	0.040	3.43	0.039	3.42	0.041	3.42	0.040

Table S2 Calculated surface $D(\vec{r})$ (bohr) and maximum ESP on σ-hole $V_{S,max}$ (a.u) of various σ-hole donors calculated at cam-B3LYP levels using various basis sets. The σ-hole is evaluated on the first atom of the molecule named highlighted in red and italic.

Molecule	6-311G(d,p)		aug-cc-pVTZ		def2-SVPD		def2-TZVP		def2-QZVP	
	$D(\vec{r})$	$V_{S,max}$	$D(\vec{r})$	$V_{S,max}$	$D(\vec{r})$	$V_{S,max}$	$D(\vec{r})$	$V_{S,max}$	$D(\vec{r})$	$V_{S,max}$
Cl-Cl	3.21	0.054	3.22	0.053	3.22	0.054	3.21	0.054	3.21	0.052
Br-Br	3.28	0.063	3.30	0.060	3.28	0.065	3.28	0.062	3.29	0.059
I-I	3.42	0.071	3.44	0.065	3.43	0.074	3.43	0.068	3.43	0.064
H-H	4.01	0.014	3.97	0.002	3.91	0.023	4.01	0.014	3.97	0.026
Cl-CH_3	3.22	0.008	3.24	0.008	3.25	0.008	3.23	0.006	3.23	0.007
Br-CH_3	3.30	0.021	3.32	0.020	3.30	0.021	3.31	0.019	3.32	0.019
I-CH_3	3.46	0.040	3.48	0.036	3.47	0.041	3.46	0.037	3.47	0.035
H-CH_3	3.28	0.021	3.29	0.022	3.25	0.019	3.29	0.021	3.29	0.022
Cl-FCH_2	3.24	0.031	3.26	0.025	3.27	0.021	3.37	0.054	3.25	0.020
Br-FCH_2	3.31	0.030	3.34	0.031	3.33	0.034	3.33	0.029	3.33	0.029
I-FCH_2	3.46	0.048	3.49	0.044	3.48	0.051	3.47	0.045	3.48	0.044
H-FCH_2	3.43	0.042	3.44	0.040	3.40	0.046	3.44	0.041	3.44	0.040

Table S3 Calculated surface $D(\vec{r})$ and minimum ESP of σ-hole acceptors C and Si in F−Cl⋯CN−R and F−Cl⋯SiN−R complexes presented in Figure 6(a). The binding energies are adopted from Ref. [13].

σ-hole acceptor	Binding Energy (kcal/mol)	$V_{S,\min}$ (kcal/mol)	$D(\vec{r})$ (bohr)
SiN-F	1.900	7.334	4.323
SiN-Cl	3.420	4.953	4.330
SiN-CCH	4.090	4.359	4.324
SiN-CCF	4.210	3.467	4.328
SiN-H	6.610	-2.925	4.350
SiN-CH_3	7.770	-5.902	4.353
SiN-Li	20.60	-26.24	4.463
SiN-Na	23.93	-31.91	4.502
CN-CN	5.480	-17.16	3.558
CN-NC	5.880	-21.21	3.547
CN-NO_2	5.970	-19.07	3.544
CN-F	6.180	-25.59	3.542
CN-CF_3	8.270	-24.23	3.565
CN-Cl	8.970	-28.22	3.560
CN-Br	10.78	-29.33	3.790
CN-H	10.86	-34.10	3.596
CN-CCF	11.63	-30.67	3.564
CN-CCH	11.64	-29.78	3.562
CN-CH_3	14.13	-39.37	3.576
CN-SiH_3	15.45	-34.13	3.618
CN-Li	28.94	-58.67	3.781
CN-Na	33.40	-64.76	3.849

Table S4 Calculated minimum ESP and corresponding surface $D(\vec{r})$ of σ-hole acceptors X, in F–Br···X–R (with X = F, Cl, Br, I and R = –H, –F) complexes. The binding energies are adopted from Ref. [10].

σ-hole Donor	Binding Energy (kcal/mol)	$V_{S,\min}$ (kcal/mol)	$D(\vec{r})$ (bohr)
FH	-3.7	-20.4	2.56
FF	-1.5	-2.32	2.47
ClH	-3.9	-9.37	3.12
ClF	-2.8	-0.41	2.91
BrH	-5.0	-7.83	3.28
BrF	-4.0	0.09	3.12
IH	-6.3	-5.95	3.49
IF	-6.0	0.43	3.36

The following relation was used to predict the binding energies:

$$\mathrm{B.E} = \alpha\, D(\vec{r}) - \beta V_{\mathrm{S,min}} - \gamma$$

The fit reproduces the binding energies with $R^2 = 0.88$, RMS error of 0.53 kcal.mol^{-1}, α = -4.28 ± 0.72 kcal.mol^{-1}.bohr^{-1}, β = 0.08 ± 0.04 and γ = 9.3 ± 2.3 kcal.mol^{-1}. The relationship between the predicted binding energies and those reported in Ref. [10] is shown in Figure S5.

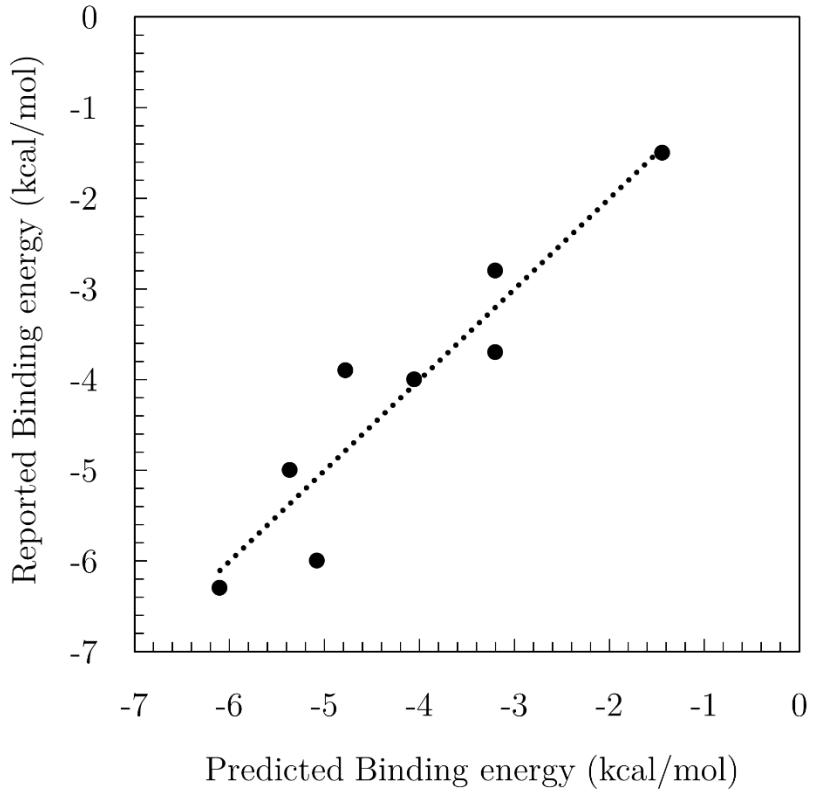

Figure S5 Relation between reported and predicted binding energies of F–Br···X–R complexes.

Table S5 Calculated maximum ESP and corresponding surface $D(\vec{r})$ of σ-hole donors complexed with formaldehyde adopted from X40 dataset. The interaction energies are taken from Ref. [14].

σ-hole Donor	Interaction Energy (kcal/mol)	$V_{S,\max}$ (kcal/mol)	$D(\vec{r})$ (bohr)
CH_3Cl	1.17	-0.909	3.28
CH_3Br	1.72	5.73	3.39
CH_3I	2.38	14.6	3.64
CF_3Cl	2.25	19.7	3.26
CF_3Br	3.1	23.9	3.38
CF_3I	4.08	32.1	3.54

Table S6 Calculated maximum ESP and corresponding surface $D(\vec{r})$ of σ-hole donors complexed with NCH adopted from XB18 and XB51 datasets. The interaction energies are taken from Ref. [15].

σ-hole Donor	Dissociation Energy (kcal/mol)	$V_{S,\max}$ (kcal/mol)	$D(\vec{r})$ (bohr)
HBr	1.41	15.8	3.361
HI	2.24	24.7	3.527
Br_2	3.63	30.1	3.347
I_2	4.03	32.8	3.485
ClBr	4.47	35.8	3.370
BrI	5.31	40.8	3.517
ClI	6.31	45.8	3.541
FBr	7.61	50.6	3.489
FI	9.45	58.0	3.751
PhBr	1.15	9.16	3.405
MeI	1.42	14.6	3.637
PhI	1.87	17.0	3.663
F_3CI	3.61	32.0	3.535
NBS	4.32	29.9	3.404
FCl	4.81	42.2	3.368
NIS	5.91	39.9	3.575

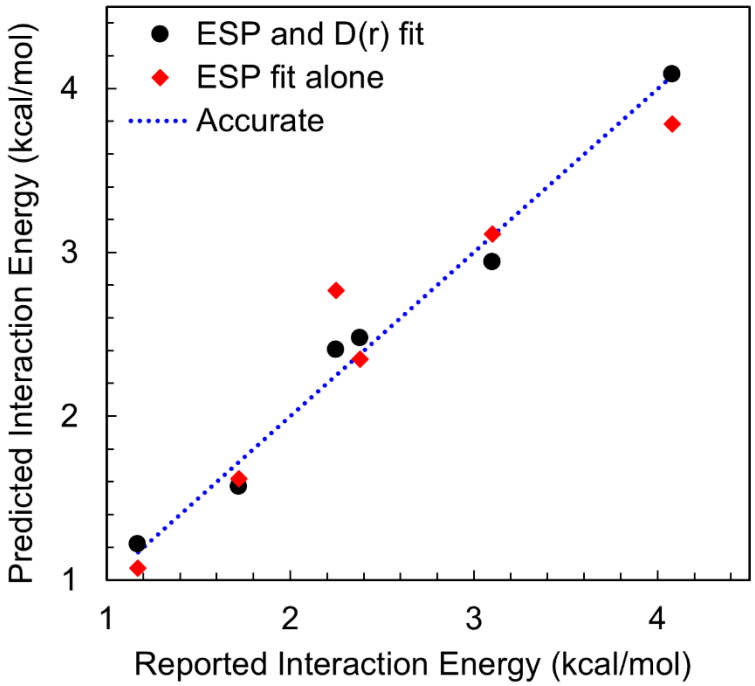

Figure S6. Relation between reported and predicted interaction energies of CH_3X and CF_3X, where X = Cl, Br, I from X40 dataset.

References

(1) *Gaussian 16 Rev. C.01*; Wallingford, CT, 2016. (accessed.

(2) Stenlid, J. H.; Johansson, A. J.; Brinck, T. σ-Holes on Transition Metal Nanoclusters and Their Influence on the Local Lewis Acidity. *Crystals* **2017**, *7* (7), 222.

(3) Stenlid, J. H.; Brinck, T. Extending the σ-Hole Concept to Metals: An Electrostatic Interpretation of the Effects of Nanostructure in Gold and Platinum Catalysis. *J. Am. Chem. Soc.* **2017**, *139* (32), 11012-11015. DOI: 10.1021/jacs.7b05987.

(4) Perdew, J. P.; Chevary, J. A.; Vosko, S. H.; Jackson, K. A.; Pederson, M. R.; Singh, D. J.; Fiolhais, C. Atoms, molecules, solids, and surfaces: Applications of the generalized gradient approximation for exchange and correlation. *Phys. Rev. B* **1992**, *46* (11), 6671-6687. DOI: 10.1103/PhysRevB.46.6671.

(5) Perdew, J. P. In *Electronic Structure of Solids '91*, Ziesche, P., Eschrig, H. Eds.; Akademie Verlag, 1991.

(6) Andrae, D.; Häußermann, U.; Dolg, M.; Stoll, H.; Preuß, H. Energy-adjustedab initio pseudopotentials for the second and third row transition elements. *Theor. Chim. Acta.* **1990**, *77* (2), 123-141. DOI: 10.1007/BF01114537.

(7) Weigend, F.; Ahlrichs, R. Balanced basis sets of split valence, triple zeta valence and quadruple zeta valence quality for H to Rn: Design and assessment of accuracy. *Phys. Chem. Chem. Phys.* **2005**, *7* (18), 3297-3305, 10.1039/B508541A. DOI: 10.1039/B508541A.

(8) Møller, C.; Plesset, M. S. Note on an Approximation Treatment for Many-Electron Systems. *Phys. Rev.* **1934**, *46* (7), 618-622. DOI: 10.1103/PhysRev.46.618.

(9) Wilson, A. K.; Woon, D. E.; Peterson, K. A.; Jr., T. H. D. Gaussian basis sets for use in correlated molecular calculations. IX. The atoms gallium through krypton. *J. Chem. Phys.* **1999**, *110* (16), 7667-7676. DOI: 10.1063/1.478678.

(10) Duarte, D. J. R.; Sosa, G. L.; Peruchena, N. M.; Alkorta, I. Halogen Bonding. The Role of the Polarizability of the Electron-pair Donor. *Phys. Chem. Chem. Phys.* **2016**, *18* (10), 7300-7309, 10.1039/C5CP07941A. DOI: 10.1039/C5CP07941A.

(11) Lu, T.; Chen, F. Multiwfn: A Multifunctional Wavefunction Analyzer. *J. Comput. Chem.* **2012**, *33* (5), 580-592. DOI: https://doi.org/10.1002/jcc.22885.

(12) Humphrey, W.; Dalke, A.; Schulten, K. VMD: Visual Molecular Dynamics. *J. Mol. Graph.* **1996**, *14* (1), 33-38. DOI: https://doi.org/10.1016/0263-7855(96)00018-5.

(13) Politzer, P.; Murray, J. S. Halogen Bonding and Beyond: Factors Influencing the Nature of CN–R and SiN–R Complexes with F–Cl and Cl2. *Theor. Chem. Acc.* **2012**, *131* (2), 1114, journal article. DOI: 10.1007/s00214-012-1114-1.

(14) Řezáč, J.; Riley, K. E.; Hobza, P. Benchmark Calculations of Noncovalent Interactions of Halogenated Molecules. *J. Chem. Theory Comput.* **2012**, *8* (11), 4285-4292. DOI: 10.1021/ct300647k.

(15) Kozuch, S.; Martin, J. M. L. Halogen Bonds: Benchmarks and Theoretical Analysis. *J. Chem. Theory Comput.* **2013**, *9* (4), 1918-1931. DOI: 10.1021/ct301064t.